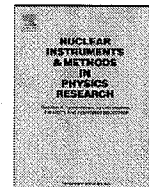




Contents lists available at ScienceDirect

Nuclear Instruments and Methods in Physics Research A

journal homepage: www.elsevier.com/locate/nima

A 3-cell deflecting RF cavity for emittance exchange experiment at ANL

Jiaru Shi^{a,b,*}, Huaibi Chen^{a,b}, Chuanxiang Tang^{a,b}, Shuxin Zheng^{a,b}, Wenhui Huang^{a,b}, John G. Power^c, Chunguang Jing^c, Kwang-Je Kim^c, Wei Gai^c, Derun Li^d

^a Department of Engineering Physics, Tsinghua University, Beijing 100084, PR China

^b Key Laboratory of Particle and Radiation Imaging of Ministry of Education, Tsinghua University, Beijing 100084, PR China

^c Argonne National Laboratory, Argonne, IL 60439, USA

^d Lawrence Berkeley National Laboratory, Berkeley, CA 94720, USA

ARTICLE INFO

Article history:

Received 14 April 2008

Received in revised form

19 September 2008

Accepted 27 September 2008

Available online 18 October 2008

Keywords:

Deflecting cavity

Emittance exchange

Coupler design

Orbit offset

ABSTRACT

An RF deflecting structure has been designed and fabricated for a transverse-to-longitudinal emittance exchange experiment at Argonne National Laboratory (ANL) [Y.-E. Sun, et al., Design study of a transverse-to-longitudinal emittance exchange proof-of-principle experiment, in: Proceedings of PAC-2007, Albuquerque, NM, USA, 2007, pp. 3441–3443 [1]]. The structure is a 1300 MHz normal conducting RF cavity consisting of three cells operating in a dipole (TM₁₁₀-like) mode. As high as 3.4 MV deflecting voltage is required for the experiment. In this paper, we present detailed RF design of the cavity, particle tracking simulations in the cavity and low power RF measurement results in comparison with numerical simulations. The cavity cell geometries (gaps in particular) are optimized to giving a zero orbit offset for particles crossing the cavity with zero-phase.

© 2008 Elsevier B.V. All rights reserved.

1. Introduction

RF deflecting cavities (deflectors) have wide applications in particle accelerators. Early applications were limited to particle separations [2–4] and bunch length measurements [3]. Recent applications or proposed applications include luminosity upgrade for high energy colliders (KEK-B factory, the Large Hadron Collider (LHC) at CERN and International Linear Collider (ILC)) [5–9]; generation of short X-ray pulses in light sources (the Advanced Light Source at Lawrence Berkeley National Laboratory, the Advanced Photon Source at Argonne National Laboratory (ANL)) [10–13]; beam diagnostics in longitudinal phase space [14,15] and emittance exchanges.

1.1. The deflecting cavity

Deflecting cavity is commonly referred as an RF cavity operating in a dipole mode. For an ideal pillbox dipole cavity, a charged particle passing the cavity on-axis receives a net transverse kick from magnetic fields only. Practically, a cavity has to have a beam iris, therefore a TE₁₁₁-like mode is mixed in near the iris region. For a properly designed deflecting cavity with

π phase advance, the transverse kicks from electric fields (near iris region) and magnetic fields (in the middle region of the cavity) add up. In addition, it is worthy of pointing out that the dipole mode in a deflecting cavity is not the fundamental mode. Moreover, for a cylindrical symmetric cavity, there are two degenerate dipole modes. Depending on applications, impedances from the fundamental mode, unwanted dipole and higher order modes have to be damped to an acceptable level specified by beam requirements, and the cavity could be either normal conducting (NC) or superconducting (SC).

The most noticeable NC deflecting RF cavities are the “LOLA” series developed at Stanford Linear Accelerator Center (SLAC) [2,3] for application in particle separation in the 1960s. The same structure is now being used in Linac Coherent Light Source (LCLS) at SLAC for beam diagnostic [14,15]. In the mean time, there are other NC structures being proposed or under research and development for longitudinal phase-space characteristic of the beams [16,17].

Progress in SC RF technology and its applications have developed rapidly in recent years. A notable example is the choice of the SC RF technology for ILC [18]. Recently the SC crabbing (or deflecting) cavities have been successfully installed and commissioned at KEK-B Factory Collider for luminosity upgrade [7]. Applications of more SC deflecting (or crabbing) cavities have been proposed. These proposals include SC crabbing cavity for the ILC and LHC luminosity upgrades [8,19]; short X-ray pulse generation for light sources [11,20–23].

*Corresponding author.

E-mail addresses: shijiaru00@mails.tsinghua.edu.cn, shijiaru00@mails.thu.edu.cn (J. Shi).

1.2. Emittance exchange

The next generation of forefront accelerator applications place increasing demands on the 6D phase space of the accelerated beam. While these demands can be met by reducing the overall 6D phase space of the beam, it is becoming increasingly difficult to do so due to fundamental physics limits like space charge compensation and photocathode optical properties. An alternative strategy, called beam phase space manipulation, is based on the observation that some accelerator applications can benefit from a repartitioning of the 6D phase space.

Recently, a phase space manipulation technique, transverse-to-longitudinal emittance exchange, was theoretically and numerically investigated. It has shown that using this technique is capable of improving the performance of the Free Electron Laser (FEL) [24–26]. A demonstration experiment to test the emittance exchange concept is under development at the Argonne Wakefield Accelerator (AWA) facility at ANL. The emittance exchange experiment consists of two identical doglegs (a pair of dipole magnets separated by a drift length) and a 1300 MHz deflecting RF cavity in between. The deflector works in a TM_{110} -like mode, and delivers a phase dependent transverse momentum kick to the particles within the bunch. The center of the bunch passes the cavity at zero-phase of the magnetic field, and therefore it does not undergo a net deflection, while the rest of the bunch (head and tail) are deflected transversely in different directions. The transverse deflection depends approximately linearly on the phase of the magnetic field when the bunch length is much shorter than RF wavelength.

A 1300 MHz NC deflecting cavity consisting of three cells has been proposed for the emittance exchange experiment at ANL. The cavity operates in a pulsed standing-wave (SW) mode with π phase advance at the lowest (TM_{110} -like) dipole mode. To achieve the required 3.4 MV deflecting voltage, 4.2 MW peak RF power is needed. Particle tracking simulations have been conducted to study the beam dynamics in the deflecting cavity. It was found that for particles even with zero-phase crossing still receive an offset at the cavity exit. A preliminary theory was developed to understand this phenomena [27], and will be discussed in detailed in Section 2. Nevertheless, this offset can be eliminated by optimizing the end cell length appropriately, which has been confirmed through numerical simulations. The RF power coupler is designed to be at critical coupling using CST Microwave Studio code in time domain [28,29].

This paper begins with a review of the basic properties of the deflecting cavity, definitions of deflecting cavity parameters, and analysis of the motion of a particle in an ideal pillbox cavity in Section 2. In Section 3, we present numerical simulations of the particle trajectory inside the deflecting cavity that includes the adjustment of the cavity geometry for eliminating the orbit offset of the zero-phase particles. Section 4 presents the coupler design. The cavity fabrication and low power microwave measurement results are given in Section 5.

2. Beam dynamics in deflecting cavity

2.1. Deflecting voltage and transport matrix

The transverse deflecting voltage in an RF cavity can be calculated by longitudinal voltage, namely simply integrating the longitudinal electric field off-axis over the cavity according to the Panofsky–Wenzel theorem [30,31]:

$$V_{\text{def}} = \left| -\frac{j}{\kappa} \frac{\partial V_z}{\partial y} \right| = \frac{1}{\kappa y_0} \left| \int_{-L/2}^{L/2} E_z(0, y_0) e^{-jkz} dz \right| \quad (1)$$

where $\kappa = \omega/c$ is the wave number, $\omega = 2\pi f$ is the angular frequency, L is the cavity length. For simplicity, we have assumed that the deflection is in y -direction in Eq. (1). Following the cavity shunt impedance definition for an accelerating cavity, the cavity shunt impedance for a deflecting cavity is defined as

$$\left(\frac{R}{Q} \right)_{\perp} = \frac{V_{\text{def}}^2}{\omega U} = \frac{\left| \int_{-L/2}^{L/2} E_z(0, y_0) e^{-jkz} dz \right|^2}{\omega U (\kappa y_0)^2} \quad (2)$$

where U is the stored energy of the dipole mode in the cavity.

The time varying RF field in the cavity gives a phase-dependent transverse momentum kick to the particles in a bunch. The kick voltage depends on longitudinal position of the particle in the bunch. The reference particle (center of the bunch) should always be at zero phase in the emittance exchange experiment. When bunch length is much shorter than λ , the RF wavelength, the transverse deflection angle $\Delta y'$ depends on approximately linearly with longitudinal coordinate s_0 .

$$\Delta y' = \frac{eV_{\text{def}} \sin \kappa s_0}{W} \approx \frac{\kappa eV_{\text{def}} s_0}{W} \quad (3)$$

where e is the elementary charge and W is the beam energy.

In (y, y', s, δ) phase space, using the thin lens approximation, the transport matrix of a deflecting cavity can be written as

$$\begin{bmatrix} y \\ y' \\ s \\ \delta \end{bmatrix} = \begin{bmatrix} 1 & 0 & 0 & 0 \\ 0 & 1 & D & 0 \\ 0 & 0 & 1 & 0 \\ D & 0 & 0 & 1 \end{bmatrix} \times \begin{bmatrix} y_0 \\ y'_0 \\ s_0 \\ \delta_0 \end{bmatrix} \quad (4)$$

where D is the deflecting strength of the cavity and defined in Refs. [24,26] as

$$D = \frac{eV_0}{aW} \quad (5)$$

where V_0 is the longitudinal voltage at off-axis displacement of a . It can also be expressed by the deflecting voltage using Eq. (1) as

$$D = \frac{\kappa eV_{\text{def}}}{W} \quad (6)$$

The deflecting strength is independent of the transverse position a . The transport matrix from the entrance to the exit of the cavity is given by

$$M = M_{L/2} M_C M_{L/2} \quad (7)$$

where M_C is the matrix in Eq. (4) and $M_{L/2}$ is the matrix of the $L/2$ drifting space. The vertical position at the exit of the cavity y_f will be

$$y_f = y_0 + Ly'_0 + \frac{LD}{2} s_0 = y_0 + \frac{L}{2} (y'_0 + y'_f) \quad (8)$$

where $y'_f = y'_0 + Ds_0$ is the angle at exit of the cavity. Nevertheless, numerical particle tracking studies show that there is an offset even for a reference particle with $y_0 = 0$, $y'_0 = 0$ and $s_0 = 0$, which is not predicted by Eq. (8).

2.2. Particle traveling through a pillbox deflecting cavity

Let us start with analytical analysis by first examining the beam dynamics in an ideal pillbox cavity. For pure TM_{110} mode, the amplitude of the transverse magnetic field on axis can be written as $B_x(x=0, y=0, z) \equiv B_0$. For an incident particle traveling through the cavity near axis at the speed of $v = c$, its motion follows the equation of

$$\frac{dp_y}{dz} = -eB_0 \sin[\kappa(z - s_0)] \quad (9)$$

where p_y is the y -component of the momentum. For a cavity in π -mode, the cavity length $L = \lambda/2$. Let $z = 0$ be the center of the cavity, the deflecting angle at position z can be expressed as

$$\begin{aligned} y'(z) &= y'_0 + \frac{cp_y(z)}{W} = y'_0 + \frac{-ecB_0}{W} \int_{-L/2}^z \sin(\kappa z - \kappa s_0) dz \\ &= y'_0 + \frac{ecB_0}{\kappa W} [\cos(\kappa z - \kappa s_0) + \sin \kappa s_0]. \end{aligned} \quad (10)$$

Therefore, the deflecting angle and the transverse displacement at the exit of the cavity, i.e. $z = L/2$ are given by

$$y'_f = y'_0 + \frac{2ecB_0}{\kappa W} \sin \kappa s_0 \quad (11)$$

$$y_f = y_0 + \int_{-L/2}^{L/2} y'(z) dz = y_0 + Ly'_0 + \frac{ecB_0}{\kappa W} \left[\frac{2 \cos \kappa s_0}{\kappa} - L \sin \kappa s_0 \right]. \quad (12)$$

Let us further substitute B_0 with the deflecting voltage V_{def} in the cavity, Eqs. (11) and (12) can be re-written as

$$y'_f = y'_0 + \frac{eV_{\text{def}}}{W} \sin \kappa s_0 \quad (13)$$

$$y_f = y_0 + \frac{L}{2} (y'_0 + y'_f) + \frac{eV_{\text{def}}}{\kappa W} \cos \kappa s_0. \quad (14)$$

In comparison with the thin lens approximation result in Eq. (8), there is an extra term, $(eV_{\text{def}}/\kappa W) \cos \kappa s_0$ responsible for the non-zero residual orbit offset when y_0 , y'_0 and s_0 are all zeros. This offset becomes negligible when the deflecting voltage is much smaller than the beam energy, which is the case for deflecting/crabbing cavity applications for high energy colliders and light sources.

Numerical simulations have been carried out to verify the analytical analysis of the ideal pillbox cavity. Particle's trajectories (transverse displacements) are numerically tracked for different initial phases ($\phi = -\kappa s_0$). The simulation results are shown in Fig. 1. For the simulations, a drift space is added intentionally before and after the cavity to amplify the effects from the residual orbit offset.

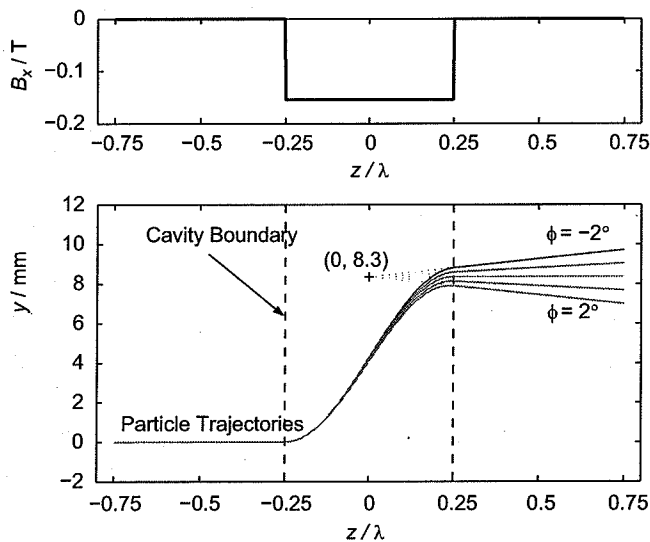


Fig. 1. Magnetic field (top) and simulated particle trajectories (bottom) in an ideal pillbox cavity with drifting space. Parameters used in the simulations: V_{def} equals; 3.4 MV and We equals; 15.5 MeV. The resulting orbit offset with respect to the reference particle is 8.3 mm, agree with the analytical calculation from Eq. (14).

3. The deflecting cavity design

To produce the required 3.4 MV deflecting voltage for the emittance exchange experiment and consider available RF source at AWA in ANL, a 1300 MHz 3-cell NC deflecting RF cavity has been chosen. For the experiment, it is not necessary to damp the lower and higher order modes in the cavity. However, the required dipole polarization must be maintained. This can be achieved by introducing necessary geometry perturbation to the other dipole polarization. In addition to meeting the requirement for the deflecting voltage, the 3-cell cavity design also gives flexibilities for eliminating the residual orbit offset by optimizing the two end cells. The 3-cell cavity design involves iterations between beam dynamics and RF cavity simulations.

3.1. Optimization of the 3-cell cavity geometry

A 3-cell NC SW cavity structure has been chosen for the emittance exchange experiment. It is unnecessary to damp the LOM and HOM for this application. The cavity design starts with a parameterized two-dimensional cylindrical symmetric structure, as shown in Fig. 2. The middle cell has a gap of $\lambda/2$ to give a π phase advance. The two end cells are identical, their gaps are adjusted by minimizing the orbit offset for reference particles. The cavity design involves iterations between beam dynamics and RF simulations until the following criteria are met: (a) minimum residual orbit offset for reference particles; (b) for the required 3.4 MV deflecting voltage, keeping the peak electric and magnetic fields below 100 MV/m and 100 kA/m, respectively; (c) flat field distribution on axis. Table 1 lists the main cavity parameters and simulation results.

As the 3-cell cavity is coupled together electromagnetically, the field amplitude in each cell depends not only on its resonant frequency, but also the coupling with adjacent cells and the beam pipe. In order to obtain a flat field distribution at 1300 MHz for the π mode, the whole 3-cell cavity with adequate long beam pipes must be included in the simulations. The radii of each cell, b_e and b_m are being adjusted to obtain the field flatness at 1300 MHz of the π mode while keeping the beam iris the same. Fig. 3 shows the simulated field distribution on axis, together with the beam dynamics simulation of vertical displacements of y and deflecting angle y' along the axis for beam with phase from -2° to 2° . The residual orbit offset for reference particles is minimized to zero by varying the gap d_e of the end cells (to be discussed below).

3.2. The cavity cell optimization and tuning study

In order to find the cavity geometry that gives zero orbit offset and flat field distribution at 1300 MHz for the π mode, simulations are carried out to scan b_e and d_e for a given b_m . Figs. 4 and 5 show an example of this simulation study results for $b_m = 134.1$ mm.

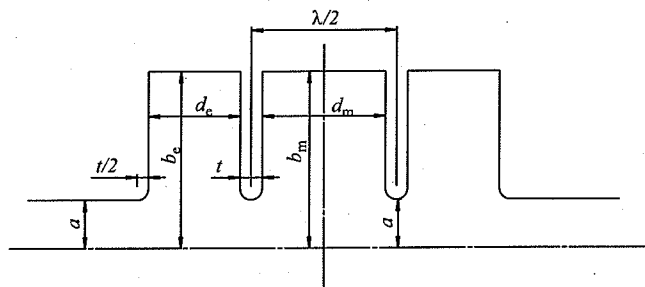


Fig. 2. 2-D Geometry of the 3-cell deflecting cavity.

Table 1
Main cavity parameters and simulation results of the 3-cell cavity.

a	36.5 mm	Q_0	2.0×10^4
b_m	134.38 mm	$(R/Q)_z$	165 Ω
b_e	133.52 mm	R_i	3.3 M Ω
d_m	94.43 mm	P_{in}	4.2 MW
d_e	51.42 mm	V_{def}	3.4 MV
f	20.88 mm	E_{max}	46 MV/m
Frequency of the working π mode			1300.00 MHz
Frequency of $\pi/2$ -like mode			1309.77 MHz
Frequency of 0-like mode			1334.03 MHz
Freq. of unwanted polarization π mode			1308.16 MHz

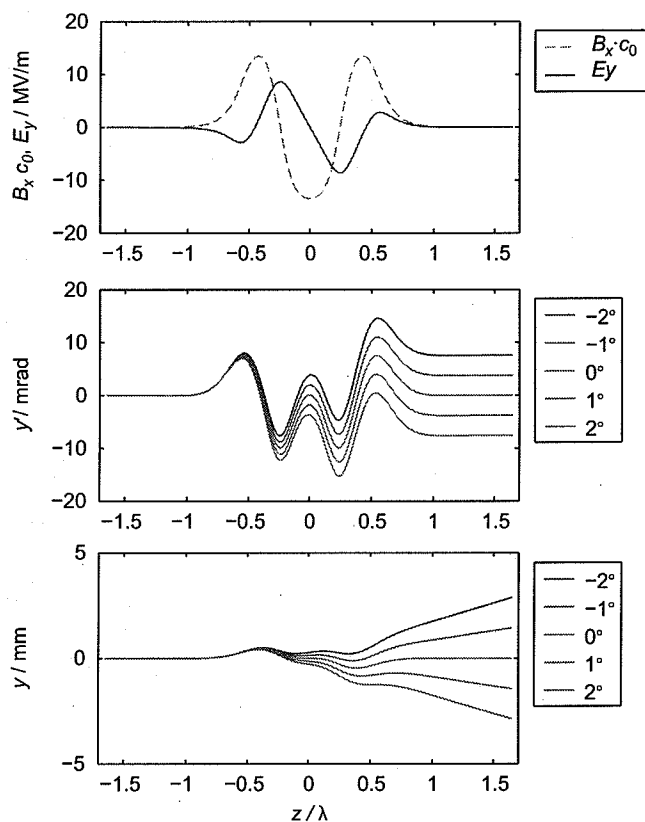


Fig. 3. Field distribution of B_x and E_y on axis, and one-dimensional particle tracking simulation results based on the fields.

The radius of the end cell b_e is tuned for field distribution while the end cell length d_e is varied to minimize the orbit offset for the reference particles. For each set of (d_e, b_e) , both the field flatness $B_{x,max,m}/B_{x,max,e}$ and vertical offset y of the reference particles are calculated and plotted in Figs. 4 and 5, respectively.

In order to find geometry parameters of b_e and d_e that give zero offset and flat field distribution at the same time, we combine and the simulation results in Figs. 4 and 5 and plot the results for zero-offset and flat field distribution only in Fig. 6, where the intersection point is the solution.

RF power is fed to the cavity in the middle cell through a coupling slot on the equator (to be discussed in Section 4). Therefore d_m , the radius of the middle cell has to be tuned later to obtain $f = 1300$ MHz at π mode.

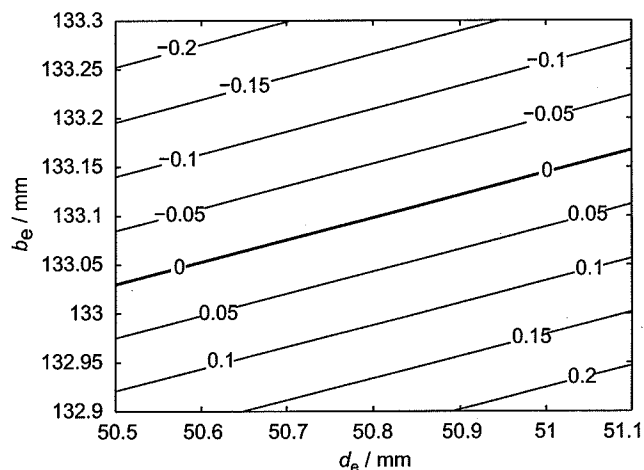


Fig. 4. Contour plot of the vertical offset y (mm) versus (d_e, b_e) .

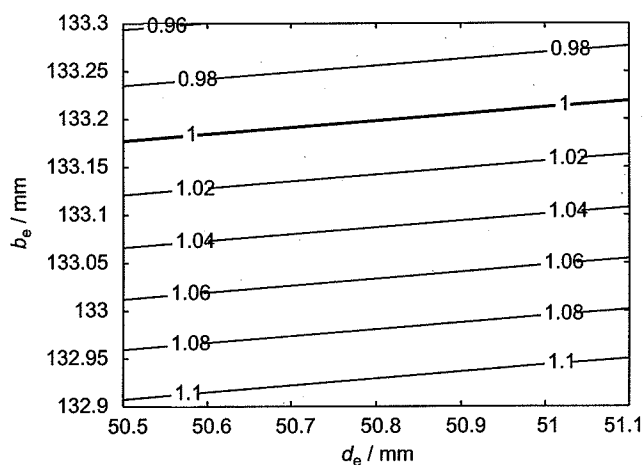


Fig. 5. Contour plot of the field flatness $B_{x,max,m}/B_{x,max,e}$ versus (d_e, b_e) .

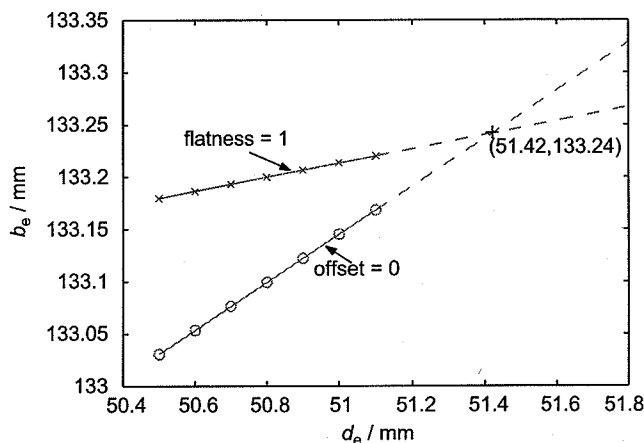


Fig. 6. Contour plots of zero-offset and flat-field distribution versus (b_e, d_e) where the intersection point at (51.42-mm, 133.24-mm) is the solution for zero-offset and flat-field distribution at the same time.

Sensitivity of the orbit offset due to machining tolerance or tuning and field flatness is studied through numerical simulations. A typical machining tolerance of 0.01 mm and 4% or better

field flatness are assumed. The simulation results are summarized in Eqs. (15)–(17).

$$\Delta y \approx 0.147 \times \Delta d_e \quad (15)$$

$$\Delta y \text{ (mm)} \approx 0.025 \times \Delta \text{Flatness (\%)} \quad (16)$$

$$\Delta \text{Flatness (\%)} \approx -37 \times \Delta b_e \text{ (mm)} \quad (17)$$

The orbit offset due to the machine tolerance is small. The field flatness needs to be tuned to be better than 2% by tuners.

In addition, the frequency shift due to temperature variation is given by

$$\Delta f_0 \text{ (kHz)} \approx -21.6 \times \Delta T \text{ (}^\circ\text{C)} \quad (18)$$

where ΔT is the temperature rise and Δf_0 is the frequency shift.

3.3. Polarization alignment holes

For a cylindrical symmetric cavity, there are two degenerate dipole modes. To break the degeneracy while keeping the needed polarization mode at the resonant frequency, two circular coupling slots (holes) are introduced on the cavity disks (walls between cells) at $(x, y) = (\pm 80, 0)$ mm with a radius of 20 mm, as shown in Fig. 7. As a result, the frequency of the working dipole mode is being pulled down while the unwanted mode frequency being shifted up. The radii of the cells have to be adjusted to bring the resonant frequency back to 1300 MHz. In addition, these coupling slots (holes) ensure and lock the dipole polarization directions. Numerical simulations show the frequency separation between the two dipole modes is 8 MHz.

4. Power coupler design

Two modules, Eigen-mode and Transient Solver of Microwave Studio code have been used for the coupler design. Q_0 is computed using the Eigen-mode Solver while the external Q_{ext} is being simulated in Transient Solver [29].

The coupler is composed of a rectangular waveguide attached to the equator of the middle cell and an opening, a rounded rectangular slot on the equator. For a brazed structure, we have assumed and should expect to achieve better than 90% of the simulated Q_0 . To calculate the external Q , field monitors are placed in each cell to record field amplitude as a function of time. Therefore both the field decay (due to external coupling of the RF coupler) and field balance between cells can be recorded. Once the designed Q_{ext} is found, the radius of the middle cell has to be adjusted again to tune the resonant frequency back to 1300 MHz. Table 2 lists the coupling slot dimensions and final cell radii for Q_{ext} of 17 700.

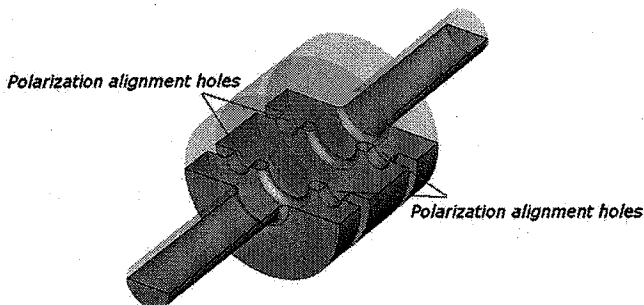


Fig. 7. The CSTMWS™ 3-cell cavity model with circular coupling slots (alignment holes) to lock the dipole polarization directions and break the degeneracy.

Table 2
Parameters of the coupler.

d_{in}	133.34 mm	Slot length	59.2 mm
b_e	133.52 mm	Slot width	30.0 mm
Q_{ext}	17 700	Slot height	145.0 mm

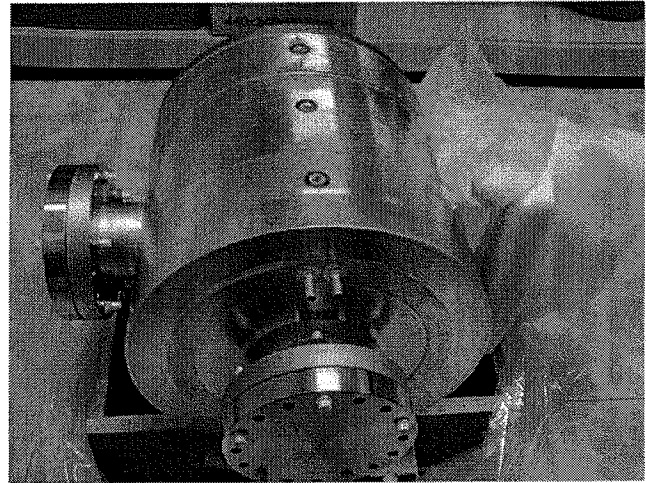


Fig. 8. Cavity after final brazing.

Table 3
The measured RF parameters after final brazing and tuning.

π mode frequency (MHz)	Q_0	Q_{ext}
1299.91	19 570	16 160

5. Cavity fabrication and preliminary measurement

The cavity is made from solid oxygen free copper (OFC) by machining. The microwave measurements agree well with the simulations. The RF coupler is brazed to the middle cell first before microwave measurement and tuning, as shown in Fig. 8.

The field flatness, coupling and frequency are all tuned to specifications before final brazing. However, unexpected thermal deformations cause frequency shifts of individual cells after final brazing. Due to limited tuning range after the brazing, we are able to achieve the field flatness within $\sim 3\%$ and the frequency for π mode at 1299.910 MHz. The frequency is ~ 100 kHz lower, but can be tuned easily by temperature ($\sim 4^\circ\text{C}$). The measured RF parameters are listed in Table 3.

6. Conclusion

A 3-cell normal conducting deflecting cavity has been designed and fabricated for the emittance exchange experiment at ANL. The cavity design is optimized to minimize the residual beam orbit offset for reference particles by carefully choosing end cell gaps and balancing field flatness. Coupling slots (holes) on cavity disks are added to lock the dipole mode polarization and perturb the unwanted dipole mode. A waveguide coupler is designed to

provide a critical coupling through a coupling slot on the equator of the middle cell. Microwave measurement results agree well with simulations. The cavity has been shipped to ANL ready for high power test and the emittance exchange experiment.

Acknowledgements

This work is supported by the Department of Energy, Office of High Energy Physics at Argonne by Contract no. DE-AC02-06CH11357.

References

- [1] Y.-E. Sun, et al., Design study of a transverse-to-longitudinal emittance exchange proof-of-principle experiment, in: Proceedings of PAC-2007, Albuquerque, NM, USA, 2007, pp. 3441–3443.
- [2] O.A. Altenmueller, R.R. Larsen, G.A. Loew, Investigations of travelling-wave separators for the Stanford two-mile linear accelerator, Technical Report SLAC-PUB-017, Stanford Linear Accelerator Center, Stanford, CA, 1963.
- [3] G.A. Loew, O.H. Altenmueller, Design and application of RF separator structures at SLAC, Technical Report SLAC-PUB-135, Stanford Linear Accelerator Center, Stanford, CA, 1965.
- [4] J.D. Fuerst, et al., An RF separated kaon beam from the main injector: superconducting aspects, Technical Report FERMILAB-TM-2060, Fermi National Accelerator Laboratory, 1998.
- [5] R.B. Palmer, Energy scaling, crab crossing and the pair problem, Technical Report SLAC-PUB-4707, Stanford, CA, 1988.
- [6] K. Oide, K. Yokoya, Phys. Rev. A 40 (1) (1989) 315.
- [7] T. Abe, K. Akai, M. Akemoto, et al., Compensation of the crossing angle with crab cavities at KEKB, in: Proceedings of PAC-2007, Albuquerque, NM, USA, 2007, pp. 27–31.
- [8] F. Zimmermann, LHC upgrade scenarios, in: Proceedings of PAC-2007, Albuquerque, NM, USA, 2007, pp. 714–718.
- [9] A. Seryi, et al., Design of the beam delivery system for the international linear collider, in: Proceedings of PAC-2007, Albuquerque, NM, USA, 2007, pp. 1985–1988.
- [10] A. Zholents, P. Heimann, M. Zolotarev, J. Byrd, Nucl. Instr. and Meth. A 425 (1999) 385.
- [11] J.N. Corlett, et al., A recirculating Linac-based facility for ultrafast X-ray science, in: Proceedings of PAC-2003, Portland, OR, USA, 2003, pp. 186–188.
- [12] D. Li, J.N. Corlett, Deflecting RF cavity design for a recirculating Linac based facility for ultrafast X-ray science, in: Proceedings of PAC-2003, Portland, OR, USA, 2003, pp. 1249–1251.
- [13] M. Borland, et al., Planned use of pulsed crab cavities for short X-ray pulse generation at the advanced photon source, in: Proceedings of PAC-2007, Albuquerque, NM, USA, 2007, pp. 1127–1129.
- [14] P. Emma, J. Frisch, P. Krejcik, A transverse RF deflecting structure for bunch length and phase space diagnostics, Technical Report LCLS-TN-00-12, Stanford Linear Accelerator Center, Stanford, CA, USA, 2000.
- [15] R. Akre, et al., A transverse RF deflecting structure for bunch length and phase space diagnostics, in: Proceedings of PAC-2001, Chicago, IL, USA, 2001, pp. 2353–2355.
- [16] D. Alesini, et al., Nucl. Instr. and Meth. A 568 (2006) 488.
- [17] R.J. England, et al., Commissioning of the UCLA neptune X-Band deflecting cavity and applications to current profile measurement of ramped electron bunches, in: Proceedings of PAC-2007, Albuquerque, NM, USA, 2007, pp. 4135–4137.
- [18] G. Burt, et al., Power coupler for the ILC crab cavity, in: Proceedings of PAC-2007, Albuquerque, NM, USA, 2007, pp. 2212–2214.
- [19] R. Calaga, et al., Small angle crab compensation for LHC IR upgrade, in: Proceedings of PAC-2007, Albuquerque, NM, USA, 2007, pp. 1583–1585.
- [20] D. Robin, et al., Generation of picosecond X-Ray pulses in the ALS using RF orbit deflection, in: Proceedings of PAC-2005, Knoxville, TN, USA, 2005, pp. 3659–3661.
- [21] J. Shi, et al., A three-cell superconducting deflecting cavity design for the ALS at LBNL, in: Proceedings of PAC-2005, Knoxville, TN, USA, 2005, pp. 4287–4289.
- [22] J. Shi, et al., Chin. Phys. C 32 (03) (2008) 205.
- [23] G. Waldschmidt, et al., Status of RF deflecting cavity design for the generation of short X-Ray pulses in the advanced photon source storage ring, in: Proceedings of EPAC-2006, Edinburgh, Scotland, 2006, pp. 3460–3461.
- [24] M. Cornacchia, P. Emma, Phys. Rev. ST: Accelerators and Beams 5 (2002) 084001.
- [25] K.-J. Kim, A. Sessler, AIP Conf. Proc. 821 (2006) 115.
- [26] P. Emma, et al., Phys. Rev. ST: Accelerators and Beams 9 (2006) 100702.
- [27] D. Edwards, Notes on transit in deflecting mode pillbox cavity, unpublished.
- [28] D. Li, R. Rimmer, Calculation of external coupling to a single cell RF cavity, in: Proceedings of LINAC-1998, Chicago, IL, USA, 1998, pp. 977–979.
- [29] J. Shi, et al., Comparison of measured and calculated coupling between a waveguide and an RF cavity using CST microwave studio, in: Proceedings of EPAC-2006, Edinburgh, Scotland, 2006, pp. 1328–1330.
- [30] M. McAshan, R. Wanzenberg, RF design of a transverse mode cavity for kaon separation, Technical Report FERMILAB-TM-2144, Fermi National Accelerator Laboratory, 2001.
- [31] M.J. Brooman, Using the Panofsky–Wenzel Theorem in the analysis of radio-frequency deflectors, in: Proceedings of PAC-1993, Washington, DC, USA, 1993, pp. 800–802.